Microchimica Acta (2020) 187:590
https://doi.org/10.1007/s00604-020-04573-4

ORIGINAL PAPER

Surface plasmon resonance biosensor using hydrogel-AuNP supramolecular spheres for determination of prostate cancer-derived exosomes

Wenqin Chen[1] · Jia Li[1] · Xiaotong Wei[1] · Yunpeng Fan[1] · Husun Qian[1] · Siqiao Li[2] · Yu Xiang[3] · Shijia Ding[1,2]

Received: 13 July 2020 / Accepted: 25 September 2020

Abstract

Based on the hydrogel-AuNP supramolecular sphere (H-Au), a label-free and real-time surface plasmon resonance imaging biosensor has been developed for highly sensitive and specific determination of prostate cancer cell-derived exosomes. After integrating the signal amplification effect of the mass cumulative hydrogel and the LSPR effect of AuNPs with high specific aptamer, the SPRi biosensor for exosome detection exhibited a wide linear range from 1.00×10^5 to 1.00×10^7 particles/mL with a limit of detection of 1.00×10^5 particles/mL. Most importantly, with a strong correlation between the SPRi signal and the t-PSA value measured by the clinical chemiluminescence immunoassay, this biosensor displayed excellent practicability for human serum analysis, which exhibits great potential applications in disease diagnosis and bioanalysis.

Keywords Exosomes · Surface plasmon resonance imaging (SPRi) · Hydrogel-gold nanoparticles (hydrogel-AuNPs) · Tumor diagnosis · Prostate-specific antigen (PSA)

Introduction

According to the Global Burden of Disease (GBD), there are more than one-fifth of new prostate cancer cases occurred in the USA in 2017, the increasing incidence rate makes it a higher prevalence disease than lung cancer [1, 2]. In addition, prostate cancer can not only cause complications such as acute seminal vesiculitis but also easily lead to bone metastasis, fracture, paraplegia, and even life-threatening [3]. Nowadays, the detection of serum prostate-specific antigen (PSA) is widely used in clinics, which is principally based on chemiluminescence immunoassay to test the content of PSA and related factors in patient serum, providing references for subsequent diagnosis [4]. In spite of this, the deficiencies of low specificity, sensitivity, and high false positive make the method full of controversy. What's worse, the detection threshold of PSA is also questioned [5]. Under these circumstances, there is no doubt that the introduction of an alternative approach to overcome the existing shortcomings and realize effective screening of prostate cancer has become one of the difficulties to be solved by researchers.

Exosomes are one of the new tumor markers sought after by researchers in recent years, which has given impetus to the publication of numerous literature on exosomes and tumors [6–8]. It is undeniable that the production, content, and function of exosomes do have a profound impact on the occurrence and development of tumors [7]. What's more, the amount of exosomes secreted by cancer cells far exceeds that of normal cells, and some exosomes have cancer-specific markers on their membrane, which explain why it is possible to monitor the occurrence of cancer by analyzing exosomes [8].

Currently, several widely used exosome detection methods include fluorescence [9], flow cytometry (FCM) [10],

Wenqin Chen and Jia Li contributed equally to this work.

Electronic supplementary material The online version of this article (https://doi.org/10.1007/s00604-020-04573-4) contains supplementary material, which is available to authorized users.

✉ Shijia Ding
dingshijia@163.com

[1] Key Laboratory of Clinical Laboratory Diagnostics (Ministry of Education), College of Laboratory Medicine, Chongqing Medical University, Chongqing 400016, China

[2] Chongqing Engineering Research Center for Criminal Investigation Technology, Chongqing Medical University, Chongqing 400016, China

[3] The Department of Clinical Laboratory, The First Affiliated Hospital of Chongqing Medical University, Chongqing 40016, China

Published online: 06 October 2020

nanoparticle tracking analysis (NTA) [11], surface plasmon resonance imaging (SPRi) [12, 13], and so on [14]. Among them, SPRi has attracted much attention because of its unique characteristics such as monitoring the reaction that happened on chip by real-time capturing of the resultant refractive index change [15]. In SPRi detection, DNA probes or antibodies modified on the gold chip surface can capture the targets through specific chemical bonds to form polymers with increased mass. A short time later, the change of refractive index caused by the binding process can be detected by a charge-coupled detector and in the meantime, the sensing image can be output [16]. Since the sensitive area of SPRi detection is within 200 nm on the chip surface [17], particles with a diameter less than 200 nm, just like exosomes, perfectly meet the requirement of this technology. Also, it is worth mentioning that as an optical platform, the signal output performance of SPRi is more stable than that of other platforms, exhibiting better photostability [15, 16].

Encouraged by the advantages of SPRi, researchers have successfully exerted a variety of strategies to detect biomolecules such as DNA [18], microRNA [19], and protein [20]. Unfortunately, the weakness of this method is that the sensitivity needs to be improved when exploited to detect trace target substances in complex samples. Then, the combined application of different signal amplification strategies, including enzyme catalysis [21, 22], nanomaterials [23, 24], and DNA nanotechnology [25–27], with this technique, has arisen and thrived. As one of the pioneers and outstanding representatives of DNA nanotechnology, DNA hydrogel, an aqueous two-dimensional or three-dimensional cross-linked network polymer, has shown broad application prospects in the field of nanotechnology and biomedicine, etc. [25]. Surprisingly, the structural controllability and variability of hydrogel material satisfy the mass-sensitive characteristic of SPRi detection [26, 27]. Hence, various kinds of hydrogel materials were investigated and utilized to improve the performance of SPRi biosensors. For instance, the gradient hydrogel matrix exhibited excellent properties of reducing nonspecific binding in SPRi biosensor applications [28]. Thermoresponsive hydrogels were applied to realize the active control of SPRi biosensor [29]. And, responsive thin hydrogel layers prevented the skin barrier effect to obtain a quick responding of SPRi detection [30]. Most importantly, the self-assembly of DNA chains to generate multi-layered porous hydrogels supplies the abundant loading sites for AuNPs to improve the signal response of SPRi detection through the LSPR effect [18–20]. Benefiting from the porous structure and large specific surface area of hydrogels, AuNPs are embedded in them by Au-S bond, which not only avoid agglomeration but also achieve effective amplification of the SPR signal.

In this study, we conceived a label-free, real-time SPRi biosensing strategy for sensitive detection of prostate cancer exosomes based on H-Au assembled by multi-layered porous hydrogels and AuNPs. Numerous of AuNPs were orderly and precisely positioned at the nanoscale grids of hydrogel spheres, and then, the greatly enhanced SPRi response can be observed for the mass cumulative hydrogels and LSPR effect of AuNPs [31]. In particular, we successfully realized the sensitive detection of exosomes in clinical samples, demonstrating good clinical applicability of this strategy.

Experimental

Reagents and materials

$HAuCl_4 \cdot 4H_2O$ was purchased from Sinopharm Chem Co., Ltd. (Shanghai, China, https://www.sinoreagent.com). 6-Mercapto-1-hexanol (MCH) was obtained from Sigma-Aldrich (St. Louis, USA, https://www.sigmaaldrich.com). Fetal bovine serum (FBS) and Dulbecco's Modified Eagle Medium (DMEM) were offered by Gibco (Gaithersburg, MD, USA, https://www.thermofisher.com). N-Hydroxysuccinimide (NHS) and N-(3-(dimethylamino) propyl)-N′-ethylcarbodiimide hydrochloride (EDC) were purchased from Alfa Aesar (Massachusetts, USA, https://www.alfaaesar.com). Tris(2-carboxyethyl)phosphine (TCEP) was provided by Aladdin Biochemical Technology Co., Ltd. (Shanghai, China, https://www.aladdin-e.com). Phosphate buffer (PBS) and bovine serum albumin (BSA) were supplied by Thermo Fisher Scientific (Wilmington, USA, https://www.thermofisher.com). Terminal transferase (TDT) was obtained from New England Biolabs Co., Ltd. (Beijing, China, https://www.neb.uk.com). Carboxyl-modified magnetic beads were offered by Chengdu Organic Chemicals Co. Ltd., Chinese Academy of Sciences (Chengdu, China, https://www.cocc.com). GelRed nucleic acid stain was acquired from SenBeiJia Biological Technology Co., Ltd. (Nanjing, China, https://www.sbjbio.com). All the chemicals used were of analytical reagent grade and all the HPLC-purified oligonucleotides listed in Table S1 were prepared and purified by Sangon Biotech. Co., Ltd. (Shanghai, China, https://www.sangon.com). Tris-EDTA (TE) buffer (10 mM Tris-HCl, 1 mM EDTA, pH 8.0) and TAE-Mg^{2+} buffer (40 mM Tris, 20 mM acetic acid, 2 mM EDTA, 12.5 mM Mg^{2+}, pH 8.0) were utilized for the dissolution and hybridization of all oligonucleotides, respectively. Aqueous solutions prepared by Millipore Milli-Q gradient ultrapure water system were used (Millipore Co., MA, USA, https://www.merckmillipore.com).

Instruments

SPRi measurements were conducted on a surface plasmon resonance imaging (SPRi) sensing platform built by our own laboratory. In short, at a fixed incident angle, a parallel p-polarized light emitted from a light-emitting diode (LED,

650 nm) passed through the prism/chip/flow cell assembly. Then, the reflected light was captured by a CCD detector. And, the change of refractive index caused by intermolecular interaction on the gold sensor chip was monitored in real time, accompanied by the output of sensing image for subsequent analysis. Transmission electron microscopic (TEM) image was performed with an H-7500 transmission electron microscope (Hitachi High-Technologies Co., Japan, https://www.hitachihightech.com). The gel electrophoresis was implemented on the DYY-6C electrophoresis analyzer (Liuyi Instrument Company, China, http://electrophoresis.globalimporter.com), followed by imaging on Bio-Rad ChemDoc XRS (Bio-Rad, USA, http://www.bio-rad.com). The size and morphology characterization of DNA hydrogel was processed on an atomic force microscope (AFM) (Hitachi High-Technologies Co., Japan, https://www.hitachihightech.com). Nanoparticle tracking analysis (NTA) was supported by ZetaView (Particle Metrix, Germany, https://www.particle-metrix.com). UV-Visible absorption spectra were carried out at a UV-2550 spectrophotometer (Shimadzu, Japan, https://www.shimadzu.com). The t-PSA values of clinical samples were measured by Cobas E602 (Roche, Switzerland, https://www.roche.com).

Culture of cells and isolation of exosomes

All cell lines were provided by the American Type Culture Collection (ATCC) (Rockville, USA, https://www.atcc.org). DMEM (added with 10% FBS, 1% streptomycin, and penicillin) was used for all kinds of cell culture in a sterile incubator containing 5% CO_2, at 37 °C. Cell passaging was processed when growth density reached 80%. Ultimately, the cells were starved with a serum-free medium for 48 h before the exosomes were extracted.

The exosomes were extracted from the cell culture medium according to the published literature [32]. Generally, after 48-h starvation, the cell culture medium was centrifuged (2000×*g*, 20 min; 10,000×*g*, 30 min; 100,000×*g*, 2 h. All steps were performed at 4 °C). The precipitate containing exosomes was suspended by 1× PBS and characterized by NTA. Twenty clinical samples were collected from the First Affiliated Hospital of Chongqing Medical University. And, the extraction procedures of exosomes from clinical samples were as described above.

Preparation of AuNPs and DNA hydrogel-AuNPs

AuNPs were synthesized by referring to the published literature [33]. Similarly, the preparation steps of DNA hydrogel were also learned from predecessors [25]. Subsequently, DNA hydrogel functionalized AuNPs were synthetized [33]. To begin with, according to the procedure, 200 μL thiol-modified DNA hydrogel (0.5 μM), 2 μL acetic acid buffer (500 mM, pH 5.2), and 1.5 μL TCEP (10 mM) were mixed at 25 °C for 1 h. Then, the mixture was added to a brown glass bottle containing 300 μL of AuNPs. After reaction in dark for at least 16 h, 3 μL Tris-acetate buffer (500 mM, pH 8.2) and 30 μL NaCl (1 M) were added dropwise, orderly. Stored in dark for 12 h later, the compound can be used after centrifugation (15,000 rpm, 10,000×*g*, 10 min) and PBS dispersion.

Synthesis of aptamer-magnetic bead complex

The preparation process of aptamer-magnetic bead conjugates was mainly based on previous achievements [33–35]. Firstly, 230 μL carboxyl-modified magnetic beads (particle size: 1.5 μm; concentration: 21.3 mg/mL) were washed with deionized water three times. Then, 115.1 mg NHS and 766.8 mg EDC were added to activate the magnetic beads (pH 5.5), with gently shaken at 4 °C for 2 h. Thereafter, 70 μL 10 μM amino-modified aptamer was added (pH 8.0), with gently shaken at 4 °C for at least 12 h to synthesize the aptamer-magnetic bead complex, after magnetic separation, washing the complex with 1 mL deionized water for three times to reduce nonspecific adsorption. Then, 3 × 70 μL, 10 μM DNA linkers (DLs) were added and gently shaken at 4 °C for at least 2 h. After repeating the above washing steps by deionized water, the MB-aptamer-DL complex was suspended in 1 mL deionized water and stored at 4 °C.

Fabrication of the SPRi biosensor

In the beginning, the gold sensor chip was cleaned with acetone, ethanol and deionized water orderly for 3 min each, and then dried with nitrogen. To further reduce the organic impurities on the sensing chip, it was necessary to cover the chip surface with ready-made piranha solution (VH_2SO_4:VH_2O_2 = 7:3) for 10 min, washed with deionized water and dried under nitrogen, then diluted the capture probe with a prepared solution of KH_2PO_4 (1 M) before modified on the chip, and blocked successively (1 mM MCH, 1 h; 2% BSA, 0.5 h). At last, the above cleaning and drying processes were repeated once again.

Determination of exosomes from prostate cancer cells

Different concentrations of exosomes were added into 50 μL solution of the MB-aptamer-DL complex to react at 37 °C for at least 2 h. Soon later, large amounts of DLs were released by chain replacement and suspended in the supernatant. After magnetic separation, the supernatant was covered on the surface of the gold chip and DLs hybridized with the pre-fixed capture probes. Thenceforth, TDT was added and incubated at 37 °C for 2 h to synthesize poly A tails. As soon as the fulfillment of this process, carefully washed the chip with deionized water and dried under nitrogen, which was ready for subsequent SPRi testing.

Detection process of SPRi

After the installment of the above modified gold sensor chip on the SPRi instrument, rinsed the injection tubes slowly with 1× PBS to remove impurities. When the stable baseline signal was output, the sample loading can be started (loading volume: 200 μL H-Au nanomaterial, flow rate: 50 μL/min, loading duration: 2 min and 40 s, reaction time: 1.5 h). Following the reaction, washed the gold sensor chip with PBS for about 15 min to get rid of the nonspecifically adsorbed substances. The program developed by our laboratory recorded the experimental data in real time and output the signal.

Results and discussion

Illustration of the SPRi sensor design principle

Scheme 1 showed the steps of the SPRi biosensor proposed in this study to detect exosomes. In Scheme 1a, the X hydrogel units (X1 and X2) were prepared through the denaturation and annealing process between DNA chains. Each unit contained two T_{29} terminals for poly A binding, two strands with thiol group modification for Au-S interaction, and four overhang arms for hybridization to form the network hydrogel. As shown in Scheme 1b, the PSMA (a diagnostic biomarker protein enriched in LNCaP cell and also highly expressed on the membrane surface of LNCaP cell-derived exosomes)-specific aptamer-DNA linker (aptamer-DLs) complexes were immobilized on the surface of MB [36, 37]. The introduction of target exosomes changed the structure of aptamer-DL-MB complexes. When aptamers bound to PSMA, triple DLs were released and then purified by magnetic separation to hybridize with capture probes for amplifying the signal in a concentration-dependent manner. As shown in Scheme 1c, the enzyme TDT catalyzed the formation of poly A tails at the exposed terminals of DLs, which would hybridize with synthesized H-Au by base pairing for signal amplification. Finally, the complex composed of poly A tails and H-Au would be detected with SPRi instrument. As expected, the obtained SPRi signal was proportional to the amount of released DLs, which was in strong correlation with the concentration of target exosomes as well [38]. The high molecular material H-Au had achieved efficient synergistic signal amplification in the determination of target exosomes. Therefore, this developed SPRi biosensor holds great potential in clinical applications.

TEM and NTA characterizations of exosomes

Figure 1a showed the morphological characteristics of LNCaP cell-derived exosomes observed by TEM. According to the image, the exosomes were small vesicles with concave surface and obvious double-layered membrane structure. Under the field of vision, the distribution density was moderate with a relatively uniform particle size of about 100 nm, which was tally with the descriptions of previous literature [39]. To further analyze the size distribution of exosomes and quantify the extracted samples, NTA was performed (Fig. 1b). Accordingly, the concentration of the purified exosomes was calculated to be 2.75×10^9 particles/mL, with a size distribution range from 80 to 160 nm. The characterization of AuNPs also performed by UV-visible absorption spectra; 520 nm and 525 nm were the typical absorption peaks of AuNPs and DNA hydrogel functionalized AuNPs, respectively (shown in Fig. S1C).

Feasibility of the developed biosensor

The hybrid products of DNA chains were verified by 3% agarose gel electrophoresis. As we can learn from Fig. 2A, the X1 (lane 3) and X2 (lane 6) hydrogel structural units were effectively synthesized by the hybridization of sub-chains. Ultimately, the network hydrogel nanostructure (lane 7) was successfully synthesized with the slowest mobility, which was in line with the expected results. In addition, we further characterize the morphology of hydrogel through AFM image (Fig. 2B) and again confirmed that the formation of DNA hydrogel was successful.

In subsequent experiments, we chose native polyacrylamide gel electrophoresis (PAGE) (see Fig. 2C) to demonstrate the formation of aptamer-DL complexes and TDT catalytic products, thereby further validating the feasibility of this research. As we can see from Fig. 2C, lanes 7 and 8, the aptamer-DL complexes migrated more slowly than single strands of DL1, DL2, DL3, and aptamers (lanes 1, 4, 5, and 6), accounting for the formation of aptamer-DL complexes. Additionally, lane 3 represented DLs-poly A after incubating the TDT with DLs, and lane 2 referred to capture probes/DL-poly A duplex, both of them moved much slower than others, denoting the successful formation of poly A tails. Except for that, SPRi experiments of different loading materials were performed to confirm the amplification efficacy of H-Au. As shown in Fig. 2D, after the addition of different signal amplification materials, corresponding response signals were obtained by the formation of different compound structures. Compared with the SPRi biosensor loaded with hydrogels (curve b), the one loaded with ssDNA-AuNPs (curve c) showed a clear increase in the response signal because of the LSPR effect of AuNPs could greatly enhance the signal. Notably, the signal increased much more significantly (curve d) when the SPRi biosensor was loaded with hydrogel-AuNPs, suggesting the signal amplification ability of hydrogel-AuNPs was much stronger than simply used ssDNA-AuNPs or hydrogels. Compared with hydrogels or ssDNA-AuNPs, the signals were amplified 8 times and 5 times, respectively. This interesting phenomenon revealed

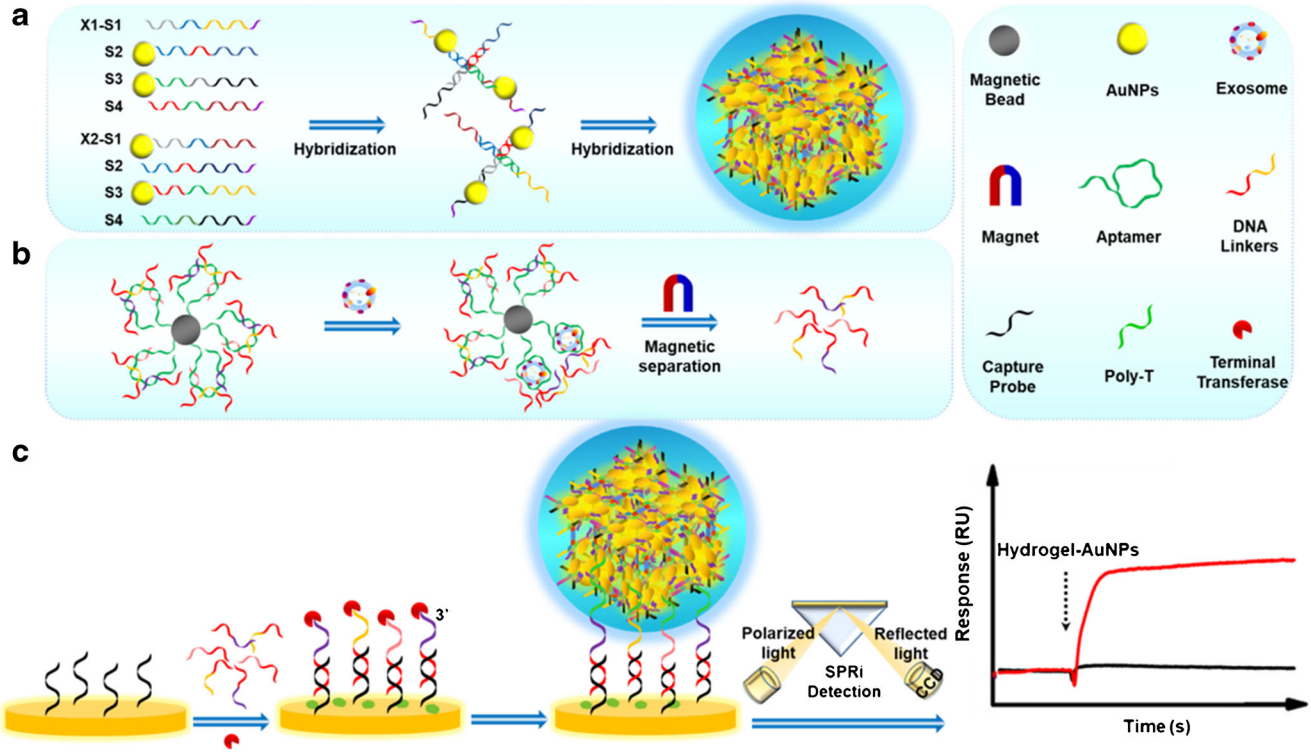

Scheme 1 Schematic illustration for the detection of tumor exosomes. **a** The synthesis of H-Au. **b** The recognition and combination of aptamers and exosomes. **c** The detection process of the released DLs by SPRi instrument.

that the SPRi sensor loaded with hydrogel-AuNPs had the most efficient signal enhancement capability because of the cooperative signal response ability of AuNPs and hydrogels. It was self-evident that H-Au exemplified a significant signal amplification effect in the sensitive detection of exosomes based on the SPRi platform.

Optimization of experimental parameters

In pursuit of ideal experimental results, we explored the optimal setting values of the parameters such as concentrations of capture probes (C_{CP}), hydrogel-AuNPs ($C_{H\text{-}Au}$), and reaction time of H-Au/DLs-poly A (see Fig. S4). The capture probes fixed on the gold sensor chip will hybridize with DLs to expose the forming sites of poly A tails, which had a non-negligible impact on the sensing signal of SPRi. Therefore, it was essential to optimize the concentration of capture probes. As shown in Fig. S4A, SPRi response rose with the increased concentration of capture probes. However, the improved spatial hindrance weakened the hybridization efficacy, and the signal decreased to a certain extent when the concentration was further raised after 2.0 μM. Hence, the concentration of capture probes was set to 2.0 μM. Next, the concentration of H-Au was also optimized in the range from 0.2 to

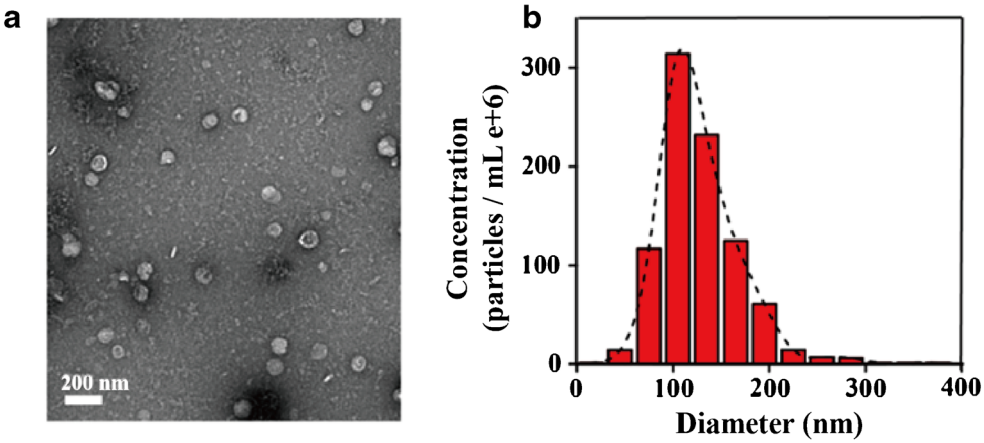

Fig. 1 The TEM image (**a**) and NTA characterization (**b**) of LNCaP cell-derived exosomes

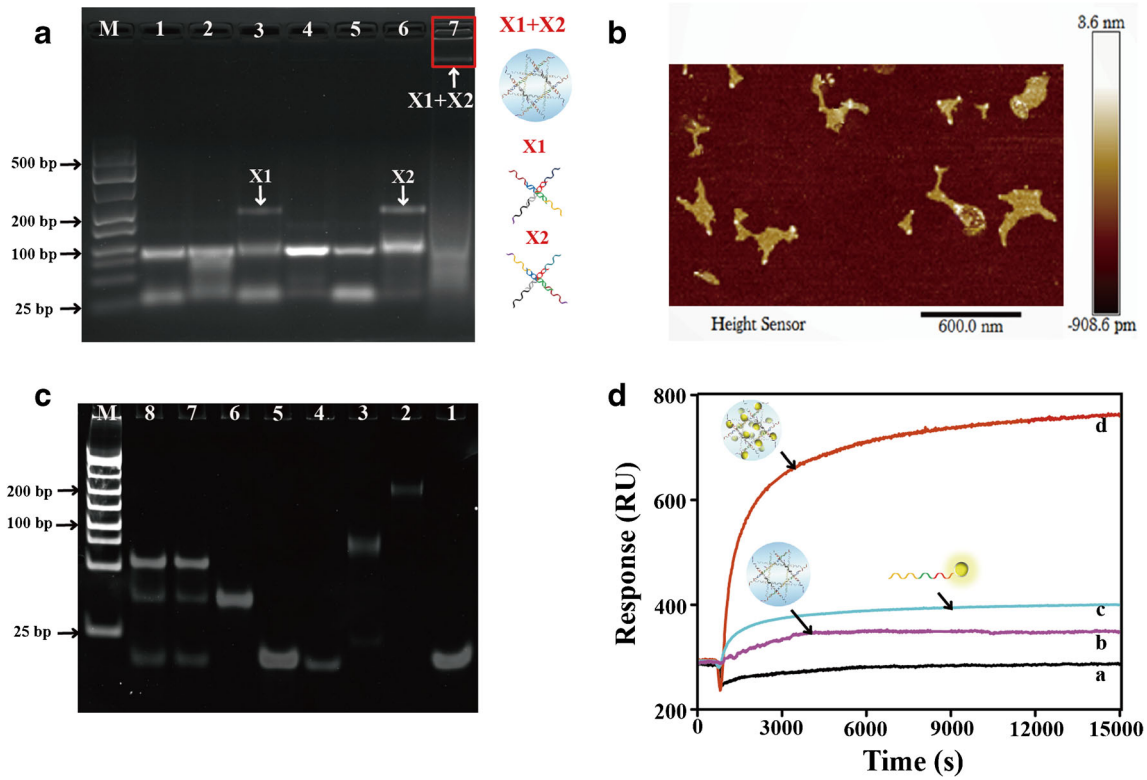

Fig. 2 (**a**) 3% agarose gel electrophoretic characterization of the DNA hybrid products. Lanes 1, 2, and 3 were the hybrid products of 2, 3, and 4 sub-chains of the X1-shaped unit, respectively. Lanes 4, 5, and 6 were the hybrid products of 2, 3, and 4 sub-chains of the X2-shaped unit, respectively. Lane 7 represented hydrogel. (**b**) AFM image of the hydrogel nanostructure. (**c**) 12% native PAGE gel of different samples. Lanes 1, 4, and 5: DNA linkers 1, 2, and 3, respectively; lane 2: duplex of capture probes/DNA linker1-poly A; lane 3: DNA linker 1-poly A; lane 6: aptamer; lanes 7 and 8: hybridization complex of aptamers and DNA linkers at different temperatures (4 °C, 37 °C). (**d**) SPR sensorgrams of different materials (0.8 μM), (a) blank, (b) hydrogels, (c) ssDNA-AuNPs, (d) hydrogel-AuNPs. All data expressed as mean ± standard variation ($n = 3$)

1.0 μM, as depicted in Fig. S4B. The SPRi response increased continuously and reached the maximum when the concentration of H-Au was 0.8 μM, supporting 0.8 μM to be chosen as the optimal concentration. Finally, the study about the optimum hybridization time of H-Au and DLs-poly A was shown in Fig. S4C. It was found that the signal ascended synchronously with the prolongation of reaction time and reached the plateau at 2 h. For that reason, the optimal reaction time was set as 2 h.

Analytical performance of SPRi biosensor

For further improvement, we took the analytical ability of this strategy into consideration. The SPR response gradually increased at an exosome concentration-dependent manner, implying the cumulative formation of the H-Au/DL-poly A duplexes (Fig. 3a). As shown in Fig. 3b, when the concentration of exosomes increased from 1.00×10^5 to 1.00×10^7 particles/mL, the corresponding SPRi signal continued to rise as well, and there was an obvious linear relationship between them. The regression equation was $Y = 4.834\ X - 16.03$ with a correlation coefficient of 0.9952, where Y and X denoted the SPR signal and the concentration of exosome, respectively. The limit of detection was calculated according to the 3σ rule to be 1.00×10^5 particles/mL, which was much lower than some reported articles (see Table 1). The high sensitivity of this assay was attributed to the combination of the surface mass of hydrogel and the LSPR effect of AuNPs, which perfectly matched with the detection feature of SPRi.

Specificity of SPRi biosensing strategy

Reflected on the fact that exosomes secreted by different cells may overlap to a certain extent in content and function, the demand for the specificity of detection methods arises accordingly. As a result, this assay was used to detect the exosomes from five different cancer cells to test whether its specificity was satisfactory. Figure 4 showed the output SPR responses of five kinds of exosomes at the concentration of 2.00×10^6 particles/mL. Apparently, only LNCaP cell-derived exosomes caused significantly higher signal, while others led to much lower signals. The appearance of such a big signal disparity was not only due to the high specificity of aptamers to target

Table 1 An overview on recently reported nanomaterial-based methods for the determination of exosomes

Detection platform	Amplification strategy	Linear range (particle/mL)	LOD (particle/mL)	Refs.
Surface plasmon resonance (SPR)	Antibody capture	8.28×10^6–3.31×10^7	8.28×10^6	[40]
Surface-enhanced Raman scattering (SERS)	Gold nanostar@raman reporter @nanoshell structures	4.00×10^4–4.00×10^{10}	2.70×10^4	[41]
Electrochemical	Gold-loaded nanoporous ferric oxide nanozymes	1.00×10^3–1.00×10^7	1.00×10^3	[42]
Colorimetric	Alternating current induced nanoshearing	2.76×10^6–4.15×10^7	2.76×10^6	[43]
Fluorescence	Graphene oxide-DNA aptamer	3.00×10^7–6.00×10^8	2.10×10^8	[44]
Electrochemical	Integrated microfluidic	1.00×10^6–1.00×10^8	1.00×10^6	[45]
Electrochemiluminescence (ECL)	Ti3C2 MXenes aptamer	5.00×10^5–5.00×10^9	1.25×10^5	[46]
Surface plasmon resonance imaging (SPRi)	Hydrogel-AuNP supramolecular sphere	1.00×10^5–1.00×10^7	1.00×10^5	This work

exosomes but also the excellent signal amplification of H-Au, which highlighted the meaning of this SPRi biosensor.

Analysis of exosomes from clinical serum

For the sake of assessing the analytical performance of this proposed method in a complex matrix, we detected cancer cell-derived exosomes in clinical samples from ten patients with prostate cancer (P1~P10) and ten healthy control subjects (H1~H10) (Fig. 5a, the blue bars). As a control, these clinical samples were tested by using the same volume under the same condition. The most worthwhile result obtained was the strongly correlated detection signals and clinical diagnostic values of the specific tumor marker t-PSA of these samples (Fig. 5a, the red bars). In contrast, the SPR signals and t-PSA detection results of the patient group were significantly higher than those of the healthy control, demonstrating that the biosensor still displayed outstanding analytical performance in serum. In other words, prostate cancer patients could be distinguished from healthy control subjects by significantly different detection signals. As shown in Fig. 5b, the calibration plot of exosome concentrations was in good linearity with the t-PSA test results of the collected serum samples. The regression equation was $Y = 1.8472\,X + 9.0183$, with a correlation coefficient of 0.9593, where Y and X represented the concentrations of exosome and the clinical test results of t-PSA, respectively since the clinical samples contain a lot of impurities, which will cause great interference in the detection of exosomes, leading to large standard deviations in experimental results. Moreover, Fig. 5c is a line graph of the SPRi signal and the t-PSA value, which more intuitively showed that the changing trend of the two is consistent. Furthermore, the calibration curve could be simulated with a typical 4-parameter model sigmoidal (Hill model): Y = bottom + (top-bottom)/(1 + 10^ ((LogEC50-X)* HillSlope)) (bottom: 8.384, top: 79.93) (Fig. 5d). Hence, the proposed method was qualified to distinguish prostate cancer patients from healthy control subjects and monitor the occurrence of tumor.

Last but not least, other than good photostability, the gold sensor chip utilized in this scheme is reusable. The analyte can be washed off the chip surface by chemical immersion, which not only increase experimental flexibility but also reduce the cost. Previous researches of our group have confirmed that unless the same chip is reused for more than 30 times, the resulting signal differences are negligible [47]. Although the advantage of this method lies in sensitive detection, there is

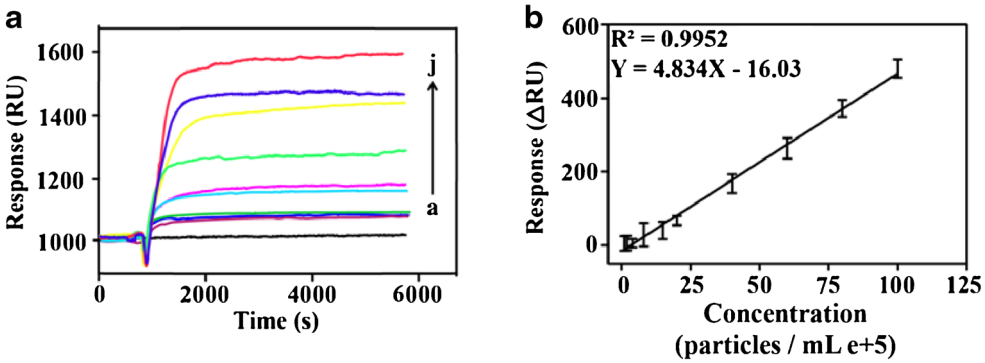

Fig. 3 SPR detection sensorgrams (**a**) and the calibration plot (**b**) for exosomes at different concentrations of 1, 2, 4, 8, 15, 20, 40, 60, 80, 100 particles/mL e+5 (from a to j). All data expressed as mean ± standard variation (n = 3)

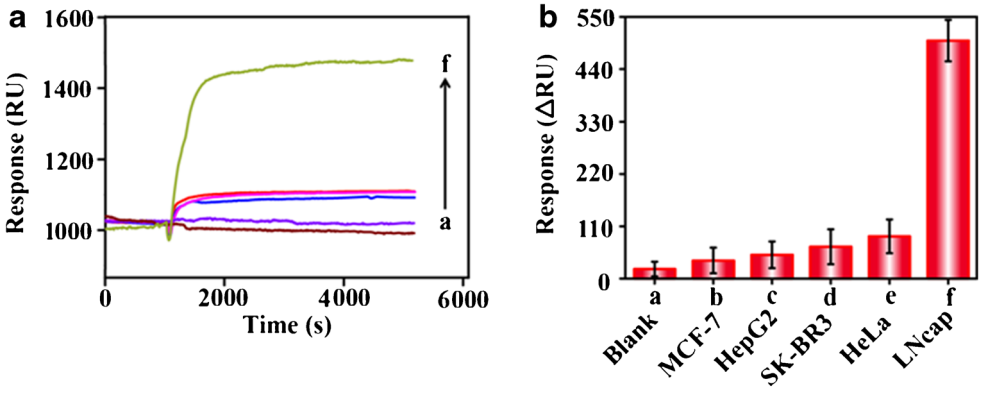

Fig. 4 SPR detection sensorgrams (**a**) and signal responses (**b**) of exosomes (2.00×10^6 particles/mL) derived from MCF-7, HepG2, SK-BR3, HeLa, and LNcap cell lines (from b to f; a represented blank). All data expressed as mean ± standard variation ($n = 3$)

still room for improvement. Therefore, in subsequent research, we will focus on shortening the detection time to further improve its clinical practicability.

Conclusion

A label-free, real-time SPRi biosensing strategy has been developed for highly sensitive and specific detection of LNCaP cell-derived exosomes based on the hydrogel-AuNP supramolecular sphere. The high sensitivity of this method is mainly attributed to the mass cumulative multilayer hydrogels and the LSPR effect of AuNPs. What's more, the developed assay has been effectively employed for the analysis of exosomes in the clinical serum of prostate cancer patients. Most significantly, there is a strong correlation between the SPRi signals and the t-PSA values measured by clinical chemiluminescence immunoassay. Benefit from that, our method is qualified to distinguish the patient group from the healthy control group, holding great potential in exosome detection based early cancer diagnosis and treatment monitoring. On this basis, we anticipate this study can provide a new alternative avenue for early screening of prostate cancer. Moreover, the integration of self-assembled DNA hydrogels with AuNPs will shed light on the development of supramolecular material-based SPRi biosensing techniques in future work.

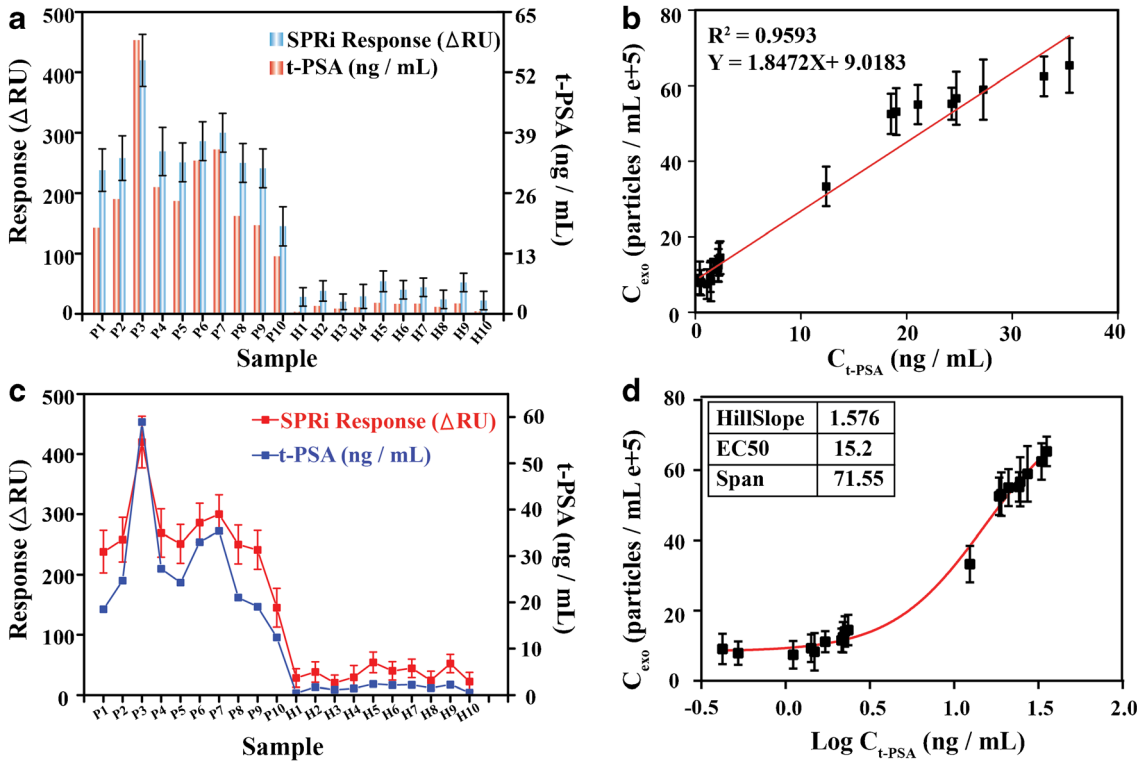

Fig. 5 **a** Analysis of exosomes of clinical samples from prostate cancer patients (P1~P10) and healthy control subjects (H1~H10) by the SPRi-based method (the blue bars) and the clinical t-PSA test results (the red bars). **b** The calibration plot of exosome concentrations with the corresponding t-PSA test results of the collected samples. **c** Line chart of the SPRi signal and the t-PSA value of the clinical samples. **d** The calibration curve simulated with 4-parameter model sigmoidal (Hill model). All data expressed as mean ± standard variation ($n = 3$)

Funding This work was supported by the National Natural Science Foundation of China (81873980, 81873972), the financial support from the National Science and Technology Major Project of the Ministry of Science and Technology of China (2018ZX10732202), and the Chongqing Medical University Graduate Talent Training Program (BJRC201908).

Compliance with ethical standards

Conflict of interest The author(s) declare that they have no competing interests.

References

1. Shoag J, Sedrakyan A, Halpern J, Hsu WC, Hu J (2017) Mp14-15 increase in the incidence of advanced prostate cancer in the United States. Int J Urol 197:e167
2. Lin L, Yan L, Liu Y (2019) Incidence and death in 29 cancer groups in 2017 and trend analysis from 1990 to 2017 from the Global Burden of Disease Study. J Hematol Oncol 12(1):1–21
3. Ost P, Bossi A, Decaestecker K, De Meerleer G, Giannarini G, Karnes RJ (2015) Metastasis-directed therapy of regional and distant recurrences after curative treatment of prostate cancer: a systematic review of the literature. Eur Urol 67:852–863
4. Cai G, Yu Z, Ren R (2018) Exciton-plasmon interaction between AuNPs/Graphene nanohybrids and CdS quantum dots/TiO2 for photoelectrochemical aptasensing of prostate-specific antigen. Acs Sens 3:632–639
5. Feng S, Lian Z, Lei J (2018) An enzyme-free immunosorbent assay of prostate specific antigen amplified by releasing pH indicator molecules entrapped in mesoporous silica nanoparticles. Anal Chem 90:7086
6. Cheng N, Du D, Wang X, Liu D, Xu W, Luo Y, Lin Y (2019) Recent advances in biosensors for detecting cancer-derived exosomes. Trends Biotechnol 37(11):1236–1254
7. Xu H, Ye BC (2020) Advances in biosensing technologies for analysis of cancer-derived exosomes. TrAC Trends Anal Chem 123:115773
8. Shao B, Xiao Z (2020) Recent achievements in exosomal biomarkers detection by nanomaterials-based optical biosensors-a review. Anal Chim Acta 1114(1):74–84
9. Sokolova V, Ludwig AK, Hornung S (2011) Characterization of exosomes derived from human cells by nanoparticle tracking analysis and scanning electron microscopy. Colloids Surf B Biointerfaces 87(1):146–150
10. Zhang P, He M, Zeng Y (2016) Ultrasensitive microfluidic analysis of circulating exosomes using a nanostructured graphene oxide/polydopamine coating. Lab Chip 16(16):3033–3042
11. Vand P, Hoekstra AG, Sturk A (2010) Optical and non-optical methods for detection and characterization of microparticles and exosomes. J Thromb Haemost 8(12):2596–2607
12. Zhu L, Wang K, Cui J, Liu H, Bu X, Ma H (2014) Label-free quantitative detection of tumor-derived exosomes through surface plasmon resonance imaging. Anal Chem 86(17):8857–8864
13. Im H, Shao H, Park YI (2014) Label-free detection and molecular profiling of exosomes with a nano-plasmonic sensor. Nat Biotechnol 32(5):490–495
14. Rupert D, Lässer C, Eldh M (2014) Determination of exosome concentration in solution using surface plasmon resonance spectroscopy. Anal Chem 86(12):5929–5936
15. Christopher L, Hu Z, Hood L (2014) SPR imaging for high throughput, label-free interaction analysis. Comb Chem High Throughput Screen 12(8):741–751
16. Campbell C, Kim G (2007) SPR microscopy and its applications to high-throughput analyses of biomolecular binding events and their kinetics. Biomaterials 28(15):2380–2392
17. Schneider A, Simons M (2013) Exosomes: vesicular carriers for intercellular communication in neurodegenerative disorders. Cell Tissue Res 352(1):33–47
18. Matsishin M, Rachkov A, Lopatynskyi A (2017) Selective amplification of SPR biosensor signal for recognition of rpoB gene fragments by use of gold nanoparticles modified by thiolated DNA. Nanoscale Res Lett 12(1):252
19. Vaisocherová H, Šípová H, Víšová I (2015) Rapid and sensitive detection of multiple microRNAs in cell lysate by low-fouling surface plasmon resonance biosensor. Biosens Bioelectron 70:226–231
20. Liu Y, Cheng Q (2012) Detection of membrane-binding proteins by surface plasmon resonance with an all-aqueous amplification scheme. Anal Chem 84(7):3179–3186
21. Karczmarczyk A, Reinerrozman C, Hageneder S (2016) Fast and sensitive detection of ochratoxin A in red wine by nanoparticle-enhanced SPR. Anal Chim Acta 937:143–150
22. Fang S, Lee H, Wark A (2006) Attomole microarray detection of microRNAs by nanoparticle-amplified SPR imaging measurements of surface polyadenylation reactions. J Am Chem Soc 128(43):14044–14046
23. Nie W, Wang Q, Zou L (2018) Low-fouling surface plasmon resonance sensor for highly sensitive detection of microRNA in a complex matrix based on the DNA tetrahedron. Anal Chem 90(21):12584–12591
24. Wu Q, Li N, Wang Y (2020) Ultrasensitive and selective determination of carcinoembryonic antigen using multifunctional ultrathin amino-functionalized Ti3C2-MXene nanosheets. Anal Chem 92(4):363
25. Guo B, Wen B, Cheng W (2018) An enzyme-free and label-free surface plasmon resonance biosensor for ultrasensitive detection of fusion gene based on DNA self-assembly hydrogel with streptavidin encapsulation. Biosens Bioelectron 112:120–126
26. Yan C, An P (2019) Concatenated catalytic hairpin assembly/hyperbranched hybridization chain reaction based enzyme-free signal amplification for the sensitive photoelectrochemical detection of human telomerase RNA. Anal Chem 91:2447
27. Ding X, Cheng W, Li Y (2017) An enzyme-free surface plasmon resonance biosensing strategy for detection of DNA and small molecule based on nonlinear hybridization chain reaction. Biosens Bioelectron 87:345–351
28. Andersson O, Larsson A, Ekblad T (2009) Gradient hydrogel matrix for microarray and biosensor applications: an imaging SPR study. Biomacromolecules 10(1):142–148
29. Toma M, Jonas U, Dostálek J (2013) Active control of SPR by thermoresponsive hydrogels for biosensor applications. J Phys Chem C 117(22):11705–11712
30. Beines P, Klosterkamp I, Menges B (2007) Responsive thin hydrogel layers from photo-cross-linkable poly (N - isopropylacrylamide) terpolymers. Langmuir 23(4):2231–2238
31. You Y, Lim S, Gunasekaran S (2020) Streptavidin-coated Au nanoparticles coupled with biotinylated antibody-based bifunctional linkers as plasmon-enhanced immunobiosensors. ACS Appl Nano Mater 3(2):1900–1909
32. Mathias R, Lim J, Ji H (2009) Isolation of extracellular membranous vesicles for proteomic analysis. Methods Mol Biol 528:227–242
33. Liu J, Lu Y (2006) Preparation of aptamer-linked gold nanoparticle purple aggregates for colorimetric sensing of analytes. Nat Protoc 1(1):246–252
34. Dong H, Chen H, Jiang J (2018) Highly sensitive electrochemical detection of tumor exosomes based on aptamer recognition-induced

multi-DNA release and cyclic enzymatic amplification. Anal Chem 90(7):4507–4513
35. Yu T, Dai P, Xu J (2016) Highly sensitive colorimetric cancer cell detection based on dual signal amplification. ACS Appl Mater Interfaces 8(7):4434–4441
36. Liu T, Mendes DE, Berkman CE (2014) Functional prostate-specific membrane antigen is enriched in exosomes from prostate cancer cells. Int J Oncol 44(3):918–922
37. Boyacioglu O, Stuart CH, Kulik G (2013) Dimeric DNA aptamer complexes for high-capacity-targeted drug delivery using pH-sensitive covalent linkages. Mol Ther Nucleic Acids 2(7):e107
38. Huang Z, Lin Q, Ye X (2020) Terminal deoxynucleotidyl transferase based signal amplification for enzyme-linked aptamer-sorbent assay of colorectal cancer exosomes. Talanta 2020(218):121089
39. Lee J, Kim J, Kwon M (2015) In situ single step detection of exosome microRNA using molecular beacon. Biomaterials 54: 116–125
40. Sina A, Vaidyanathan R, Wuethrich A (2019) Label-free detection of exosomes using a surface plasmon resonance biosensor. Anal Bioanal Chem 411(7):1311–1318
41. Cheng B, Fei T, Cui N (2018) Highly sensitive detection of exosomes by SERS using gold nanostar@Raman reporter@nanoshell structures modified with a bivalent cholesterol-labeled DNA anchor. Analyst 143(20):4915–4922
42. Fu JL, Fang Q, Zhang T (2006) Laser-induced fluorescence detection system for microfluidic chips based on an orthogonal optical arrangement. Anal Chem 78(11):3827–3834
43. Vaidyanathan R, Naghibosadat M, Rauf S (2014) Detecting exosomes specifically: a multiplexed device based on alternating current electrohydrodynamic induced nanoshearing. Anal Chem 86(22):11125–11132
44. Wang H, Chen H, Huang Z (2018) DNase I enzyme-aided fluorescence signal amplification based on graphene oxide-DNA aptamer interactions for colorectal cancer exosome detection. Talanta 184: 219–226
45. Zhou Q, Rahimian A, Son K (2016) Development of an aptasensor for electrochemical detection of exosomes. Methods 97:88–93
46. Liu N, Ma Z (2014) Au-ionic liquid functionalized reduced graphene oxide immunosensing platform for simultaneous electrochemical detection of multiple analytes. Biosens Bioelectron 51(1): 184–190
47. Zhang D, Yan Y, Cheng W (2015) Streptavidin-enhanced surface plasmon resonance biosensor for highly sensitive and specific detection of microRNA. Microchim Acta 180(5–6):397–403